Relationship between topographic parameters and BRDF for tungsten surfaces in the visible spectrum

Mickaël Le Bohec, Roland Steiner, Hiroki Natsume, Shin Kajita, Marwa Ben Yaala, Laurent Marot, Marie-Hélène Aumeunier

Optik - International Journal for Light and Electron Optics 303 (2024) 171750

Contents lists available at ScienceDirect

Optik - International Journal for Light and Electron Optics

journal homepage: www.elsevier.com/locate/ijleo

Original research article

Relationship between topographic parameters and BRDF for tungsten surfaces in the visible spectrum

Mickaël Le Bohec [a], Roland Steiner [b], Hiroki Natsume [c], Shin Kajita [d], Marwa Ben Yaala [e], Laurent Marot [b,*], Marie-Hélène Aumeunier [a]

[a] CEA/IRFM Cadarache, 13108 Saint Paul-Lez-Durance, France
[b] Department of Physics, University of Basel, Switzerland
[c] Graduate School of Engineering, Nagoya University, Nagoya 464-8603, Japan
[d] Graduate School of Frontier Sciences, The University of Tokyo, Kashiwa 277-8561, Japan
[e] SUPA, Department of Biomedical Engineering, University of Strathclyde, Glasgow G1 1QE, UK

ARTICLE INFO

Keywords:
BRDF
Roughness
Reflectance
Tokamak
Tungsten

ABSTRACT

In metallic fusion devices, parasitic light originating from multiple reflections on the wall is a major problem for the interpretation of optical diagnostics. Strong stray light affects several optical diagnostics in ITER. One possibility to cope with this reflected light is to use photonic simulation, which can accurately predict the behavior of light within complex 3D geometry. A prerequisite is to get a good description of the reflection model, represented by the Bidirectional Reflectance Distribution Function (BRDF), based on optical measurements of in-vessel materials. To avoid complicated measurements using goniophotometer to get the BRDF, one possibility is to link surface optical properties and topography characteristics, such as roughness measurements, for example, using the classical Bennett's formula.

Measurements were performed using two experimental goniophotometers to fully characterize the BRDF of tungsten samples with different roughness values. Surface topography was measured using a three-dimensional laser scanning confocal microscope. Several parameters were extracted from these measurements including the arithmetic average roughness (R_a), the root mean square roughness (RMS), the Surface Inclination Angle Distribution and furthermore its mean value δ_m and the power spectral density (PSD). The correlations of BRDF model parameters deduced from the measurements are compared with the previous topographic parameters. The initial results on several tungsten samples show that R_a, which is the usual measure of surface roughness, is not the most suitable metric to link with the reflection behavior of the surface. In contrast, the PSD and the surface inclination angle are interesting metrics for describing the reflected light.

1. Introduction

For fusion reactors like ITER or DEMO, plasma diagnostics and wall temperature monitoring will be crucial for the safety of these devices. In these reactors as well as in JET [1], ASDEX Upgrade [2] and WEST [3,4] the reactor first wall (FW) is entirely metallic. Strong stray light produced by reflections from the metallic FW is a primary concern for diagnostics. For ITER as an example, the first wall will be composed of tungsten (W) and beryllium (Be) and stray light will affect visible spectroscopy diagnostic

* Corresponding author.
E-mail address: laurent.marot@unibas.ch (L. Marot).

https://doi.org/10.1016/j.ijleo.2024.171750
Received 24 November 2023; Received in revised form 16 February 2024; Accepted 9 March 2024
Available online 16 March 2024

systems [5,6], infrared imaging system [7], charge exchange recombination spectroscopy [8] and synthetic H-alpha [9]. Therefore, the consideration of the effect of the reflected light is required for ITER diagnostics. One approach is to quantitatively evaluate reflection effects using ray-tracing software. Photonic simulation codes were performed using the Monte Carlo ray-tracer and have already been investigated with LightTools [10,11], CHERAB [12,13], SPEOS [7,14] and Raysect [15–17]. All these ray-tracers are based on photon-material interaction models using experimental data or a model known as bidirectional reflectance distribution function (BRDF) [18]. The choice of the BRDF model and the relevance of the experimental surface measurement are constantly under discussion among the community. Moreover, it should be noted that the light reflection properties of FW will likely change after the following exposure to plasma. To explain these issues in more detail, we focus on a specific diagnostic, that is, the infrared (IR) imaging system. One way to determine the FW surface temperature is to use numerical methods to simulate the transport of IR radiation in the vacuum chamber and quantify the contributions of reflections according to the plasma scenario [19,20] [Part S3 in the supplementary file]. The optical radiative properties of materials are described through emissivity, temperature, and reflectance models, including the variables of the BRDF model. However, as previously explained, BRDFs are not thoroughly measured, and the models do not always represent the sample surface. Considering tungsten for the fusion environment, the first measurements were performed by Ben Yaala et al. and Natsume et al. [14,21,22]. The papers reported two different experimental methods to measure the BRDF. Ben Yaala used the most commonly adopted reference method i.e. comparing the reflected sample flux to a well-known reference reflectivity [14]. Natsume et al. obtained absolute measurement by taking the ratio of the reflected light's radiance to the incident light's irradiance (Supplementary Information part S4) [21]. Both references investigated BRDF model with Gaussian function and Natsume et al. also tested the microfacet model using the Trowbridge–Reitz distribution, often called GGX [23].

Another idea is to measure the emissivity, which is linked to the BRDF [Part S2 in the supplementary file] of the high-heat-load W area of the WEST reactor [24]. These measurements demonstrated a strong spatial emissivity variation from 0.05 to 0.85. The optical properties of W are likely to change after plasma exposure, and the erosion-deposition phenomenon occurring during the reactor lifetime will certainly modify the emissivity. According to Gaspar et al. low emissivity is related to the area eroded by ion bombardment and a high value on the deposition area (accumulation of FW eroded material) [24].

Coming back to the BRDF measurements and surface topography, the link between BRDF and surface roughness was already established [25,26]. The standard parameter in surface topography is the well-established arithmetic average of the absolute values of the profile height deviations from the mean line (R_a) [Equation S8]. R_a is expressed in μm or nm and contributes to the characterization of a surface in the community [14,22,24]. A few BRDF models [23,27,28] used a parameter link to the width of the reflection lobe as the roughness coefficient, which is a purely mathematical value between 0 and 1 and without dimensions. It can also be expressed as the arithmetic mean slope of a surface profile, which is the mean absolute profile slope over the measurement length (R_s), and is not limited to the range 0–1 [Equation S10]. Moreover, theoretical models relate the roughness (R_a) of a plane surface to its specular reflectance, roughness R_a and R_s to its reflectance [29], and power spectral density function (PSD) of the BRDF [30–33]. However, these models are classically used for smooth surfaces, which restricts their application and cannot describe the reflectivity of our samples (Figure S1).

In this work, we investigate the link between BRDF and the surface roughness of tungsten samples in the visible range. This work aims to study BRDF measurements using two experimental goniophotometers to fully characterize the BRDF of tungsten samples with different roughness values. From these measurements, we extracted several parameters, such as arithmetic height average roughness (R_a), arithmetic slope average roughness (R_s), root mean square height roughness (RMS), root mean square slope roughness (RMS_s), spectrally relevant roughness (σ_{rel}), Surface Inclination Angle Distribution, mean value δ_m and PSD. The correlations of the BRDF model parameters deduced from the measurements are compared with previous topographic parameters.

2. The bidirectional reflection distribution function

2.1. Definition

The bidirectional reflection distribution function [34,35] entirely describes the reflective behavior of a surface with respect to incident and reflected direction and wavelength. It is defined as the ratio between the reflected radiance $\mathrm{d}L_r(\boldsymbol{\omega}_i, \boldsymbol{\omega}_r)$ into the direction $\boldsymbol{\omega}_r$ due to the irradiation $\mathrm{d}E(\boldsymbol{\omega}_i)$ coming from $\boldsymbol{\omega}_i$ within $\mathrm{d}\omega_i$ and this same irradiation:

$$\rho''(\boldsymbol{\omega}_i, \boldsymbol{\omega}_r) = \frac{\mathrm{d}L_r(\boldsymbol{\omega}_i, \boldsymbol{\omega}_r)}{\mathrm{d}E(\boldsymbol{\omega}_i)} = \frac{\mathrm{d}L_r(\boldsymbol{\omega}_i, \boldsymbol{\omega}_r)}{L_i(\boldsymbol{\omega}_i)\cos\theta_i \mathrm{d}\omega_i} \tag{1}$$

It has the dimension of the inverse of steradians and can take values greater than 1. It obeys Helmholtz reciprocity and energy conservation [Equations S1 and S2].

The most commonly used property associated with reflections is called the directional-hemispherical reflectance $\rho'^{\frown}(\boldsymbol{x}, \boldsymbol{\omega}_i)$ [Equations S3] which is most often simply referred to as *the* reflectance. It is typically measured by using an integrating sphere. It describes the proportion of flux leaving a surface into all directions due to the irradiation coming from one direction.

2.2. Model

Several different BRDF models have been reported in the literature. The most important are the cosine lobe models [36–38], and Gaussian lobe models [27,28]. Other models are also widely used like GGX [23,39,40]. The various models are currently used

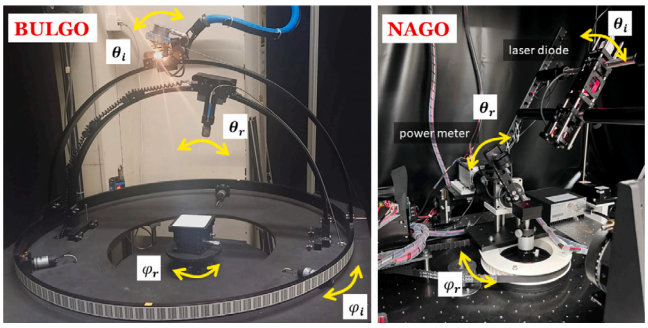

Fig. 1. Pictures of BULGO and NAGO goniophotometers.

into the micro-facet framework [41]. Their purpose is particularly to incorporate the phenomena of the evolution of the BRDF as a function of the angle of incidence as well as the visual effects due to the Fresnel coefficient (water appears as a mirror at a grazing angle and transparent otherwise). To keep things simple and because we do not focus on these phenomena, we stay outside of the micro-facet framework.

The simplest model to use is certainly the Phong model [37]:

$$\rho''(\boldsymbol{x}, \boldsymbol{\omega}_i, \boldsymbol{\omega}_r) = \rho''_d(\boldsymbol{x}, \boldsymbol{\omega}_i, \boldsymbol{\omega}_r) + \rho''_s(\boldsymbol{x}, \boldsymbol{\omega}_i, \boldsymbol{\omega}_r) \tag{2}$$

$$= k_d \frac{1}{\pi} + k_s \frac{n+2}{2\pi} \cos^n \alpha \tag{3}$$

where α is the angle between the perfect specular reflective direction and the effective reflective direction, k_d is the diffuse reflectance, i.e. the fraction of incoming energy that is reflected diffusely, k_s is the specular reflectance, i.e. the fraction of perpendicularly incoming energy that is reflected specularly and n is the specular exponent linked to the Full Width at Half Maximum (FWHM) by the empirical expression:

$$n = f(FWHM) \tag{4}$$

This model only requires 3 parameters with a clear physical meaning and the reflectance has a neat analytical expression at normal incidence:

$$\rho'^{\frown}(\boldsymbol{x}, \boldsymbol{\omega}_i) = \int_S \rho''(\boldsymbol{x}, \boldsymbol{\omega}_i, \boldsymbol{\omega}_r) \cos\theta_r \mathrm{d}\omega_r \tag{5}$$

$$= \int_S \left[k_d \frac{1}{\pi} + k_s \frac{n+2}{2\pi} \cos^n \alpha \right] \cos\theta_r \mathrm{d}\omega_r \tag{6}$$

$$= k_d + k_s \frac{n+2}{2\pi} \int_S \cos^n \alpha \cos\theta_r \mathrm{d}\omega_r \tag{7}$$

For normal incidence $\alpha = \theta_r$ so the integral equal $\frac{2\pi}{n+2}$ and

$$\rho'^{\frown}(\boldsymbol{x}, \boldsymbol{\omega}_i) = k_d + k_s \tag{8}$$

3. Topographic analysis

The usual way to describe the surface roughness is to compute the arithmetic average roughness R_a (possibly the root mean square height roughness RMS) [14] [Equations S8 and S9]. It only requires the height distribution of the surface which is easy to measure with a profilometer, confocal microscopy or atomic force microscope. But the reflection of photons on a surface is better described with the local slopes encountered because this is what determines the direction of reflection following the Snell-Descartes law. Various parameters can be computed: the arithmetic average slope roughness R_s [Equations S10], the root mean square slope roughness RMS_s [Equations S11] and the mean inclination angle:

$$\delta_m = \frac{1}{N_x N_y} \sum_{i=1}^{N_x} \sum_{j=1}^{N_y} \arctan \sqrt{\frac{\Delta z_i}{\Delta x_i}^2 + \frac{\Delta z_j}{\Delta y_j}^2} \tag{9}$$

where N_x and N_y are the number of measures in the two directions of the sample measurement plan and $\Delta z_i/\Delta x_i$ and $\Delta z_j/\Delta y_j$ are respectively the slope due to a variation of height in the x direction and the y direction. A representation of the surface inclination angle is in figure S4.

The main interest of δ_m is that it is bounded between 0 and π. It can thus be normalized $\bar{\delta}_m = \delta_m/\pi$ so that it can be used in BRDF models with a mathematical parameter used as roughness with value between 0 and 1 already commonly used in models [23,27,28].

It is also possible to take into account the spectrum of the radiation being studied. A material can be smooth at long wavelengths and rough at short wavelengths [35]. To do so, the PSD of the height distribution is produced and the relevant roughness σ_{rel} is calculated [32]:

$$\sigma_{rel} = \sqrt{2\pi \int_{f_{min}}^{f_{max}} PSD(f) f \, \mathrm{d}f} \tag{10}$$

where f_{min} and f_{max} define the range of wavelength of interest and $PSD(f)$ is the PSD at the frequency f. This makes it possible to describe the surface irregularities that are of the same order of magnitude as the radiation and that have the greatest impact on it.

To explore how the roughness of the sample affects the measured BRDF, the surface roughness of the samples was also measured using a three-dimensional laser scanning confocal microscope (3D LSCM, VK-X1100, Keyence). An objective lens of 20 times magnification was used to reconstruct the surface topography. The arithmetical mean height of the surface is calculated over an area of 531 × 708 μm^2.

4. Experimental

4.1. Setup

The BRDF is a function of four geometric variables, namely the angles defining the directions of incidence (θ_i, φ_i) and reflection (θ_r, φ_r) (see Figure 2a of Ref. [14]). The measurement of a BRDF requires a device capable of traversing all pairs of directions which is called a gonioreflectometer.

There are several types of gonioreflectometers, depending on the type of detector or the shape of the sample. The main purpose of these different versions is to reduce the measurement time which is intrinsically important. The general principle remains the same. For each pair of position of the lamp and the detector, the signal from the reflection on the sample I_{sample} is compared to a reference signal I_{ref} whose BRDF ρ''_{ref} is known. A third measurement is necessary to subtract the dark current I_{dark}, measured by obstructing the detector. If these three measurements are made at different integration times, this must be taken into account by relating each of the signals to their respective integration times (label as t_{sample}, t_{ref} and t_{dark}).

$$\rho''_{sample}(\theta_i, \varphi_i, \theta_r, \varphi_r) = \rho''_{ref}(\theta_i, \varphi_i, \theta_r, \varphi_r) \frac{\frac{I_{sample}}{t_{sample}} - \frac{I_{dark}}{t_{dark}}}{\frac{I_{ref}}{t_{ref}} - \frac{I_{dark}}{t_{dark}}} \tag{11}$$

The only BRDF easily accessible in their entirety are those of diffuse materials. In this case, it is constant whatever the angles of incidence and reflection and directly deducible from the reflectance ρ_{ref}:

$$\rho''_{ref}(\theta_i, \varphi_i, \theta_r, \varphi_r) = \frac{\rho_{ref}}{\pi} \tag{12}$$

Thus:

$$\rho''_{sample}(\theta_i, \varphi_i, \theta_r, \varphi_r) = \frac{\rho_{ref}}{\pi} \frac{\frac{I_{sample}}{t_{sample}} - \frac{I_{dark}}{t_{dark}}}{\frac{I_{ref}}{t_{ref}} - \frac{I_{dark}}{t_{dark}}} \tag{13}$$

The material used for the reference is an extremely Lambertian high-density polyethylene Spectralon©. It is a very diffuse and highly reflective standard for the 250 to 2500 nm range and its reflectance is known. The Basel University Laboratory GOniospectrophotometer (BULGO) we use is well described in Ben Yaala et al. [14] as the NAgoya GOniophotometer (NAGO) [42] and presented in Fig. 1. The 0° incidence normal reflectance was measured using a UVvis-near infrared (NIR) spectrophotometer Varian Cary 5 equipped with a 110 mm diameter integrating sphere under nearly normal incidence (3° 20′) in the wavelength range of 0.25–2.5 μm [13].

4.2. Fitting methodology

As the samples were supposed to be isotropic and to reduce the measurement time, only one incident plane was measured. The data were analyzed and fitted as shown in Fig. 2. The lower part of Fig. 2 shows an example of a Phong function in spherical coordinates view from above. The blue spot is the reflection peak related to the specular part and the pale green disk is the offset value related to the diffuse part. A cross section on the incident plane is plotted on the top graph of Fig. 2 showing the characteristic Gaussian/cosine lobe aspect.

In Fig. 3, a BRDF is plotted in one plane and the parameters of Eq. (3) are indicated. k_d is extracted from the minimal value, n is extracted from the measured fwhm and k_s is extracted from the maximal value and the n value.

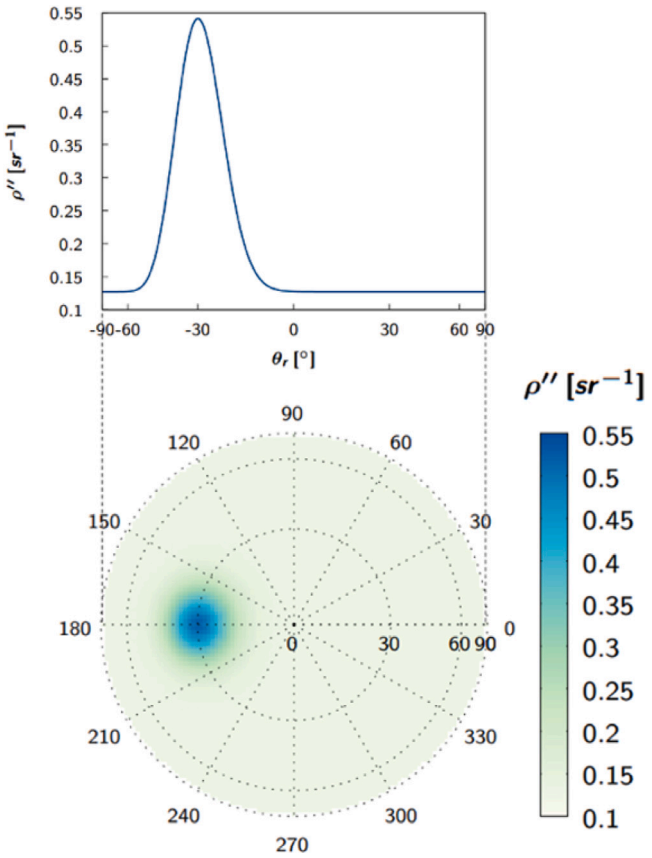

Fig. 2. Top view of a Phong function in spherical coordinates (bottom) associated to its incident plane (top).

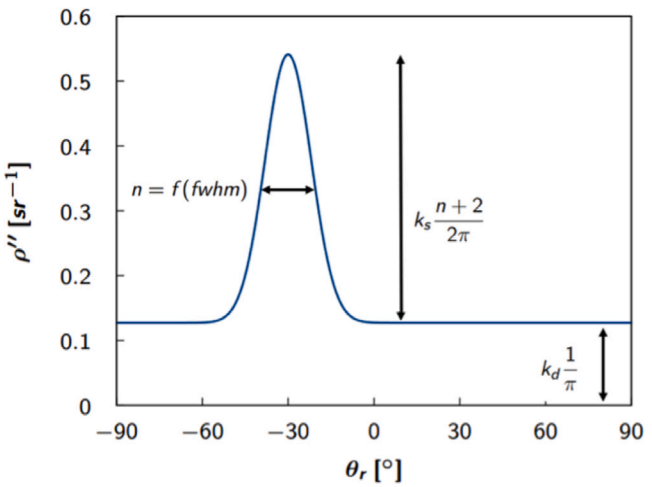

Fig. 3. Classical BRDF profile is presented and the parameters of the Phong model (Eq. (3)) are indicated.

5. Results and discussions

Optical properties and surface topography were investigated for all tungsten samples presented in Fig. 4. The samples M100-103 were described by Ben Yaala at al. [14], M104 was selected for its high roughness. Tungsten plates producted by Nilaco Corp. were used for M105-107. No additional surface treatment was added to M105, but M106 and M107 were sputtered by ions in helium and argon plasmas, respectively.

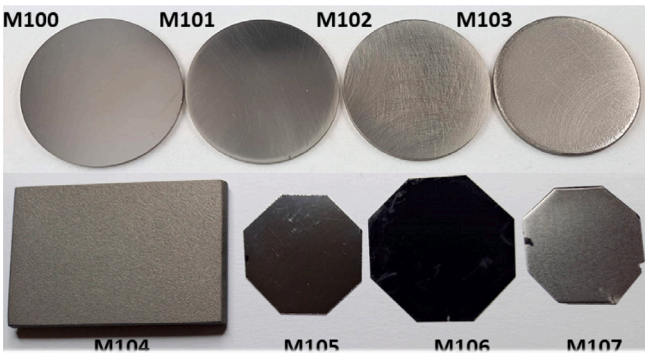

Fig. 4. Pictures of tungsten samples M100-M107.

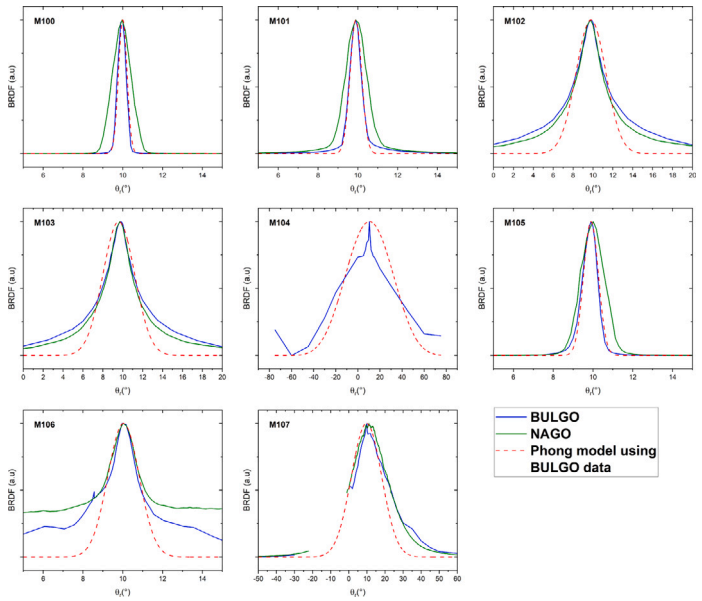

Fig. 5. Normalized BRDF of samples M100-107 measured with BULGO and NAGO. The dashed line is the Phong model fitted with BULGO data.

The BRDF was measured using both goniometers and plotted for θ_i and $\theta_r = 10$ degrees in Fig. 5. Moreover, other reflection angles (θ_r) were also measured and are presented in figure S3. From 10 to 60°, the FWHM does not vary significantly. This was also demonstrated in previous measurements of samples M100 to M103 [14] and also with beryllium samples measured with BULGO and NAGO [42].

The intensity of the BRDF was normalized for the comparison. The shape of the BRDF was similar for the two goniophotometer for all samples. The main difference is the larger FWHM for specular samples measured with NAGO, and also reported in table S1. In the case of low specular reflectivity (Fig. 6), the width of the BRDF is comparable. The data from Fig. 5 were fitted with the Phong model (Eq. (3)) and the relevant parameters k_s, k_d, n and FWHM (from Fig. 3) were extracted. Comparing optical properties measured with the spectrophotometer (Fig. 6) and the BRDF measured with BULGO, there is a linear trend between the specular reflectivity and k_s and for the diffuse reflectivity and k_d as presented in Fig. 7.

The surface topography can also be analyzed using methods of fractal geometry, such as power spectral density (PSD) functions. The PSD of a surface is a mathematical tool that decomposes a surface into contributions from different spatial frequencies (wavevectors). The PSD is the Fourier transform of the autocorrelation function of the signal, which contains just the power (and not the phase) across a range of wavevectors. This allows the identification of spatial frequencies in the signal, which provide topographical parameters like equivalent roughness, fractal dimension and Hurst exponent. The 1D PSD represents the surface height squared (roughness power) per spatial frequency. It was calculated by integrating the 2D signal over the frequential radius $f_r = \sqrt{f_x^2 + f_y^2}$ (Figure S2b). Fig. 8a displays in a log-lin plot the resulting 1D PSD profiles computed from confocal images. The 1D PSD was plotted as a function of the spatial frequency which is directly inversely proportional to the wavelength in the real space. PSD curves generally present the same characteristic shape: a response in the lower part of the spatial frequency spectrum and a

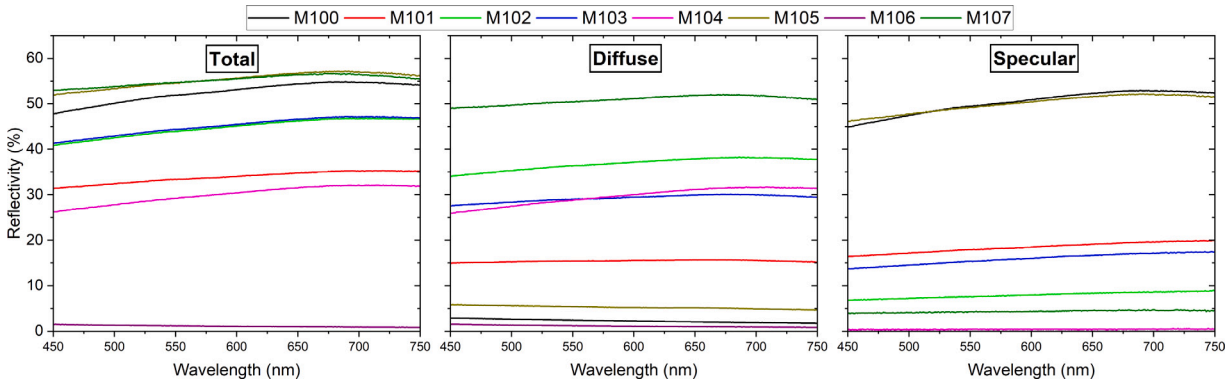

Fig. 6. Total, diffuse and specular reflectivity of all tungsten samples M100-M107.

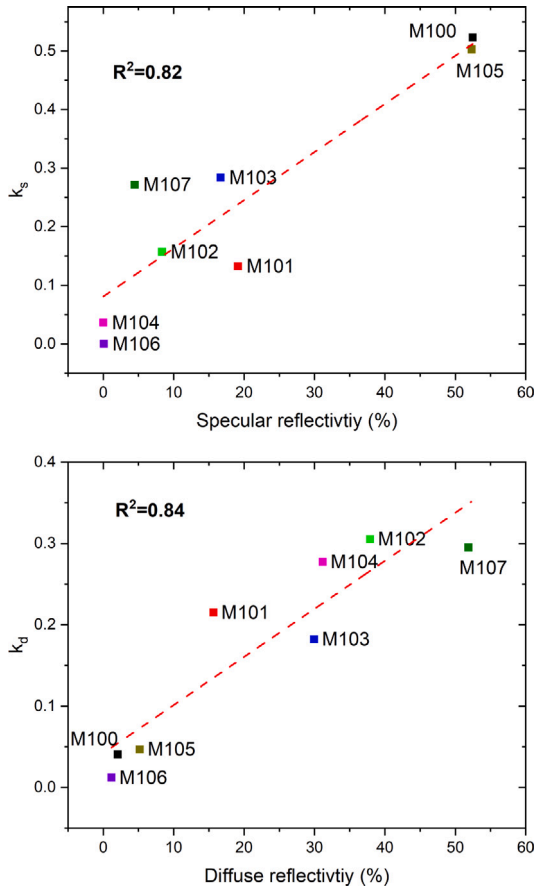

Fig. 7. k_s as function of the specular reflectivity and k_d as function of diffuse reflectivity.

power-law dependence (Supplementary Information S6) with the spatial frequency in the upper part of the spectrum corresponding to the highly correlated region.

The PSD is the two-dimensional frequency space representation of the surface topography and it is directly linked to the optical scattering distribution from the sample [44]. Harvey et al. also reported careful measurements of material surface statistics [45]. The Generalized Harvey-Shack (GHS) BRDF model was used to compute the PSD from the BRDF data. In this reference, the computed PSD using GHS theory closely matched the measured statistics of the surfaces. For our data, in the range, 1.3–2.3 μm^{-1} ($\lambda = 400-800$ nm), the 1D PSD in Fig. 8a follow the diffuse intensity (Fig. 8b) i.e. the order of the 1D PSD is the same as the diffuse reflectivity order. Only the samples M104 (pink color) do not match previous explained trend. The total reflectivity for the M104 at 600 nm

Table 1
Roughness values of parameters of samples M100-105 and M107. The sample M106 has foam structure reported in [43] and it make no sens to have roughness values.

	R_a [µm]	R_s [–]	RMS [µm]	σ_{rel} [µm]	δ_m [°]	$\bar{\delta_m}$ [–]
M100	0.021	0.041	0.031	0.021	2.374	0.026
M101	0.086	0.247	0.124	0.108	13.110	0.146
M102	0.354	0.398	0.499	0.182	19.666	0.219
M103	0.447	0.257	0.724	0.134	13.133	0.146
M104	6.404	1.165	8.342	1.636	38.988	0.433
M105	0.832	0.280	1.077	0.247	14.266	0.159
M107	0.059	0.054	0.077	0.041	3.063	0.034

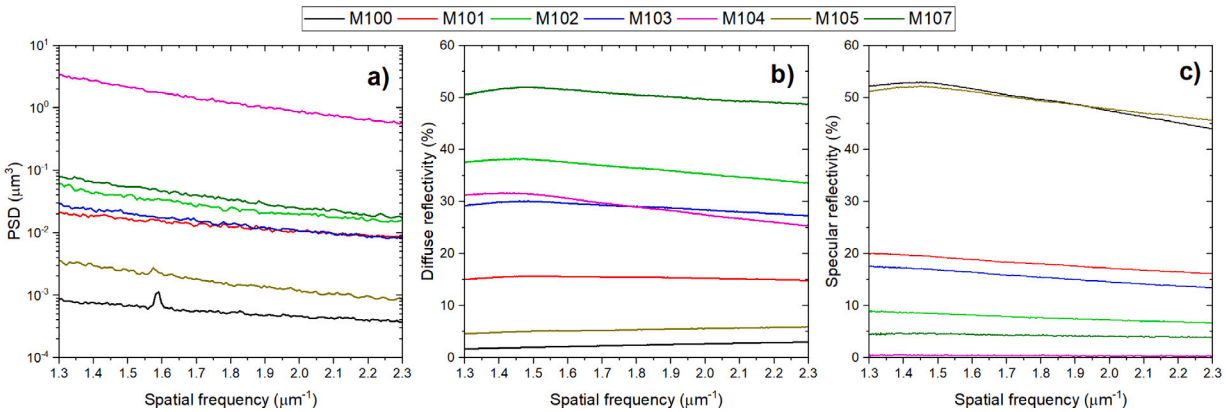

Fig. 8. (a) is power-spectra obtained using a FFT of topography image of samples M100-107. (b) diffuse, (c) specular reflectivity of the same samples.

is 30% and for a polished tungsten like M100, M105 is 55% for the same wavelength. Considering Reflection + Transmission + Absorption = 1 and assuming the metal transmission to be negligible, the absorption for M104 is around 25%. For sure, for the M104, the diffuse reflectivity cannot be higher than the total reflectivity (about 30%). However, the M102 and M107 have a total reflectivity of 45 and 55%, respectively, allowing these two samples to have a higher diffuse reflectivity than M104. Therefore, even if the roughness for M104 (Table 1) and the PSD (Fig. 8a) is logically the highest due to his topography, this led to a discrepancy in the previously explained trend. However, there is a one-to-one reverse sequential correspondence comparing the relation of the PSD and the specular reflectivity (Fig. 8c).

From the topography measurements, roughness parameters were calculated using the formula in Supplementary Information S5 and are presented in Table 1. The Phong parameters were plotted against the R_a, R_s and RMS roughness values in Fig. 9. There was no direct correlation between these roughness values and the Phong model parameters (Fig. 3), especially for samples with a high roughness value like the M104. The R^2 of the linear fit in Fig. 9 is rather low. Similarly, using the Bennett–Porteus law (Equations S15), the reflectivity of the samples was calculated using R_a from Table 1 for σ value and was plotted in figure S1. Even though the Bennett–Porteus formula is classically used [46], it failed to describe the samples' reflectivity with higher roughness. However, other topographic analyses described in part 3 use different parameters like δ_m and σ_{rel} and were also used in several Refs. [30–32,47].

Cupak et al. and also Szabo et al. recently showed that δ_m included all information on the roughness of Gaussian surfaces and is therefore well-suited as a characterization parameter, especially for surfaces with random roughness [48,49]. For example, δ_m is much better suited to categorize rough surfaces in regard to their ion sputtering behavior than the RMS roughness. They achieved this using a ray-tracing simulation code for ions which can be used for photons [50]. Moreover, in 2020, it was reported that the surface inclination angle and the micrometer-scale defects affect the BRDF distribution measured using an illumination optical system and an imaging optical system called one-shot light direction color mapping imaging system [51,52].

In Fig. 10, k_s, k_d, FWHM and n are plotted in the range of 400–800 nm as a function of the σ_{rel}, δ_m and RMS_s roughness parameters. We find a better correlation between the mean surface inclination angle distribution δ_m and the Phong parameters (k_s, k_d, FWHM and n). The figure S5 confirms this trend and the link between δ_m and k_s: the rate of occurrence of δ follows the specular reflectivity plotted in Fig. 6 and the mean value δ_m indicated in figure S5 is similarly higher for the lower specular sample. However, the link with Phong parameters is less clear with other metrics (σ_{rel} and RMS_s): we obtain an equivalent R^2 computed for R_a, R_s and RMS. The next step should be increasing the number of samples to confirm the correlation.

6. Conclusion and outlook

Surface roughness parameters including R_a, RMS, R_s, δ_m, σ_{rel} and RMS_s were calculated using topography measurements. BRDFs of tungsten samples with different roughness were measured using two experimental goniophotometers and were fitted using

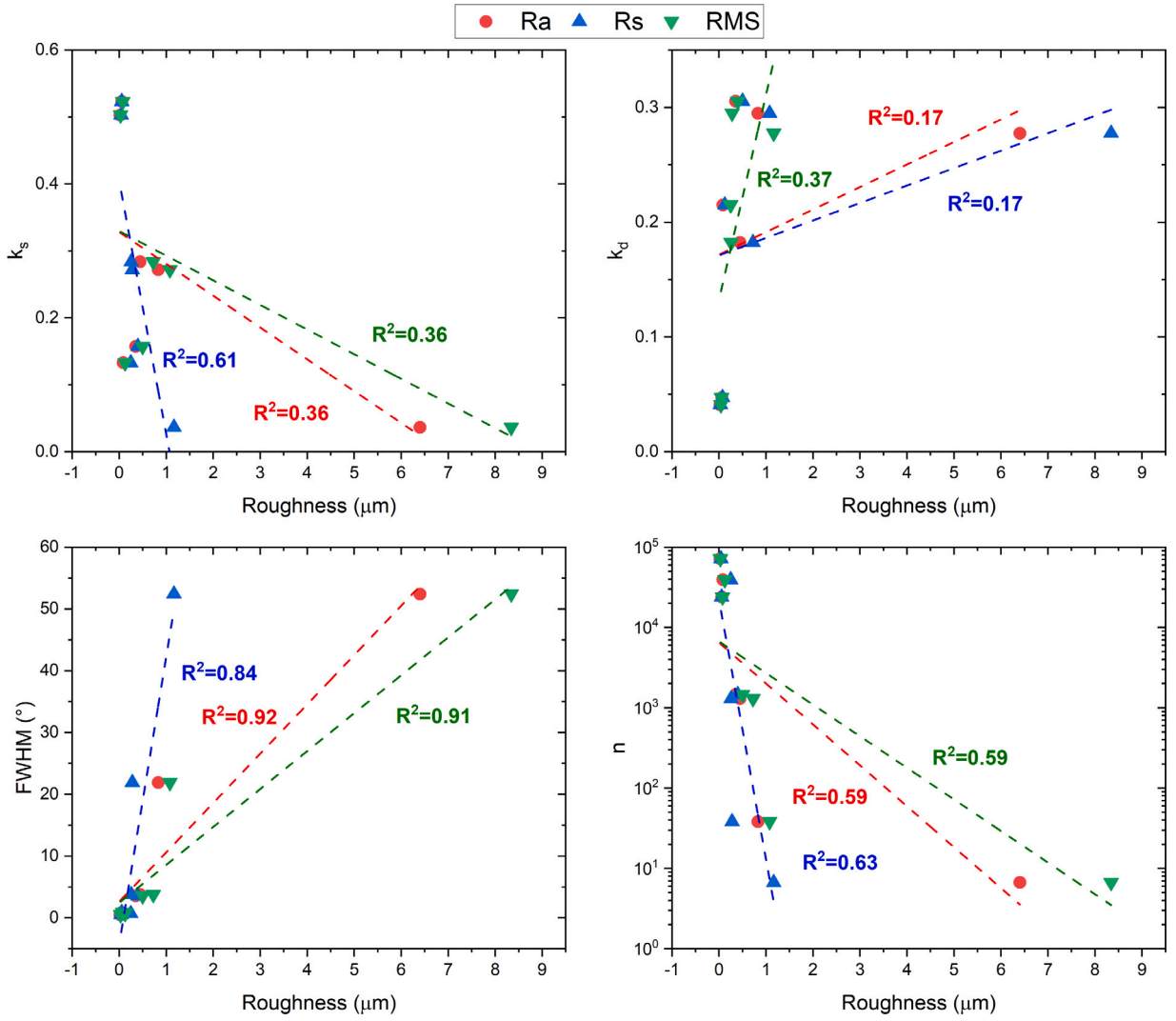

Fig. 9. k_s, k_d, FWHM and n as a function of R_a, R_s and RMS. The R^2 of the linear fit is indicated on the graphs.

the Phong model and the four parameters, k_d, k_s, n and FWHM, were obtained for all samples. The relationship between the Phong parameters k_s and k_d with the specular and diffuse reflectance, respectively, is well verified. In the scope of our paper, which aims to identify the best roughness parameters related to a BRDF model, the first results on several tungsten samples show that R_a, RMS and R_s, classically used in the community to characterize a surface, are not the most suitable metric to link the reflection behavior of the surface and topography. Even if this correlation is not perfect, on the other hand, the mean surface tilt angle distribution seems to be an interesting metric that shows a better correlation with the BRDF model (Phong parameters). The next step is to extend these studies to other samples with various roughness in order to consolidate the correlation with better statistics. As a first example, we similarly analyzed the results of 4 other samples presented by Natsume et al. [42] and then plotted in figures S6 and S7. The same trend was verified. Spectral characteristics, which were elucidated via PSD analysis, were used. PSD offers visualization of surface geometric properties at all wavelengths. Similarly, the 1D PSD follows the diffuse reflectivity trend. This is an interesting method for characterizing a surface, as topography measurements are more straightforward than BRDF measurements, especially when materials are installed in a fusion reactor. The work was carried out on tungsten surfaces, which is one material of the ITER fusion reactor and should also be verified on other material and especially on the second ITER wall material namely beryllium [42]. The next step is to investigate other theoretical models, e.g., microfacet BRDF driven by physical parameters such as microfacet normal distribution, roughness, etc [23].

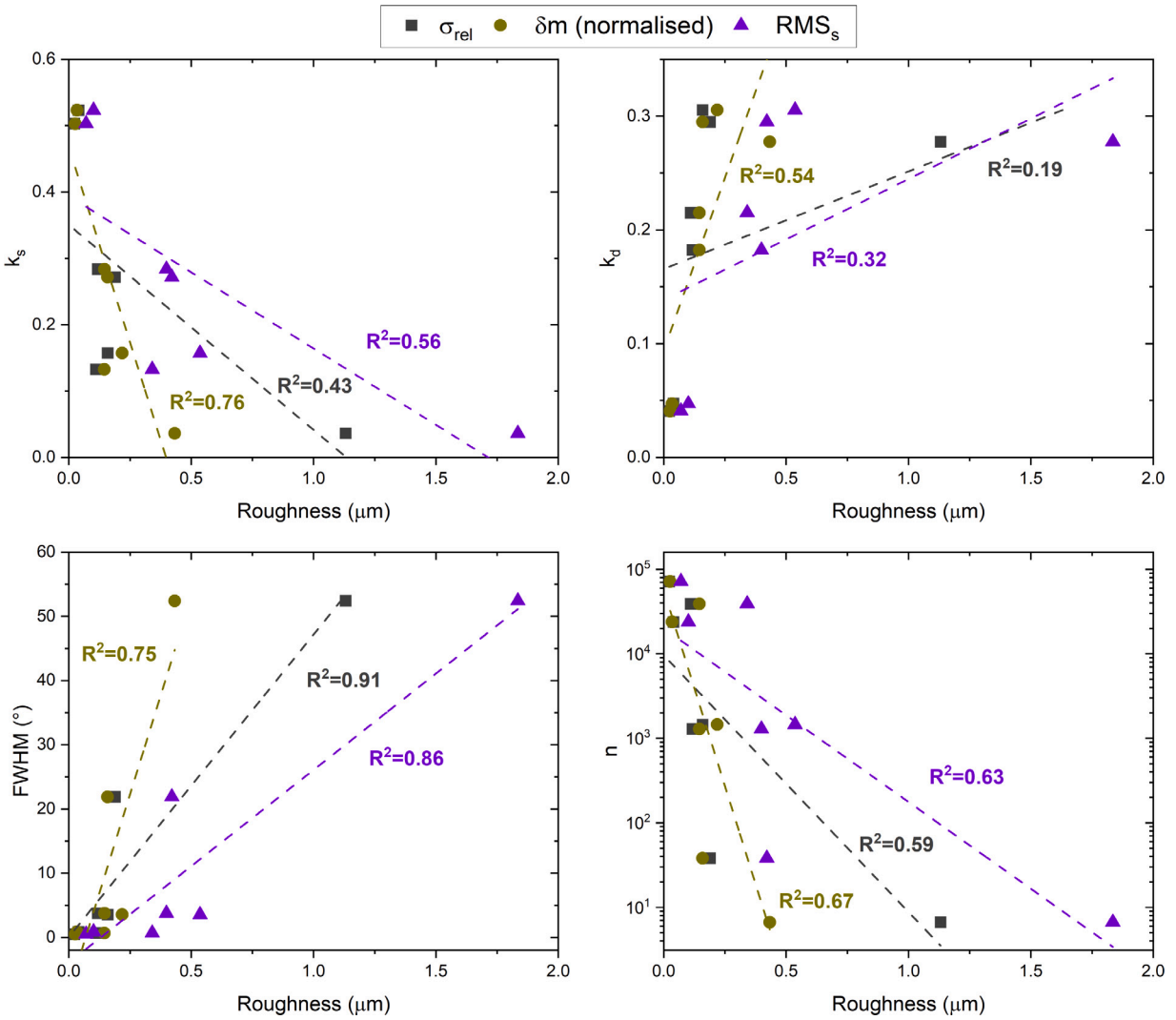

Fig. 10. k_s, k_d, FWHM and n as a function of σ_{rel}, normalized δ_m and RMS_s. The R^2 of the linear fit is indicated on the graphs.

CRediT authorship contribution statement

Mickaël Le Bohec: Writing – original draft, Visualization, Validation, Methodology, Investigation. **Roland Steiner:** Resources, Methodology, Investigation, Conceptualization. **Hiroki Natsume:** Writing – review & editing, Resources, Methodology, Investigation. **Shin Kajita:** Supervision, Project administration, Funding acquisition, Conceptualization. **Marwa Ben Yaala:** Writing – review & editing. **Laurent Marot:** Writing – review & editing, Writing – original draft, Visualization, Supervision, Funding acquisition, Conceptualization. **Marie-Hélène Aumeunier:** Writing – review & editing, Supervision, Funding acquisition, Conceptualization.

Declaration of competing interest

The authors declare the following financial interests/personal relationships which may be considered as potential competing interests: Laurent Marot reports financial support was provided by University of Basel. If there are other authors, they declare that they have no known competing financial interests or personal relationships that could have appeared to influence the work reported in this paper.

Data availability

Data will be made available on request.

Acknowledgments

This work has been carried out within the framework of the EUROfusion Consortium and has received funding from the Euratom research and training programme 2014–2018 and 2019–2020, France under grant agreement No 633053 and also via the Euratom Research and Training Programme, France under grant agreement No 101052200. Views and opinions expressed are however those of the author(s) only and do not necessarily reflect those of the European Union or the European Commission. Neither the European Union nor the European Commission can be held responsible for them. The authors would like to thank the Swiss Nanoscience Institute, Switzerland are acknowledged for their financial support. This work was supported by the Swiss State Secretariat for Education, Research and Innovation (SERI), Switzerland under contract number 22.00424.

Appendix A. Supplementary data

Supplementary material related to this article can be found online at https://doi.org/10.1016/j.ijleo.2024.171750.

References

[1] K.-D. Zastrow, S.R. Keatings, L. Marot, M.G. O'Mullane, G. de Temmerman, JET-EFDA Contributors, Modeling the effect of reflection from metallic walls on spectroscopic measurements, Rev. Sci. Instrum. 79 (10) (2008) 10F527.
[2] J. Harhausen, A. Kallenbach, C. Fuchs, the ASDEX Upgrade Team, Interpretation of D_α video diagnostics data as a contribution to plasma edge characterization, Plasma Phys. Control. Fusion 53 (2) (2011) 025002.
[3] M.-H. Aumeunier, J. Gerardin, C. Talatizi, M. Le Bohec, M. Ben Yaala, L. Marot, T. Loarer, R. Mitteau, J. Gaspar, F. Rigollet, X. Courtois, M. Houry, A. Herrmann, M. Faitsch, Infrared thermography in metallic environments of WEST and ASDEX upgrade, Nucl. Mater. Energy 26 (2021) 100879.
[4] Charly Talatizi, Marie-Hélène Aumeunier, Fabrice Rigollet, Mickael Le Bohec, Christophe Le Niliot, Albrecht Herrmann, Solving the infrared reflections contribution by inversion of synthetic diagnostics: First results on WEST, Fusion Eng. Des. 171 (2021) 112570.
[5] Shin Kajita, Evgeny Veshchev, Steve Lisgo, Roger Reichle, Robin Barnsley, Michael Walsh, Andrey Alekseev, Aleksey Gorshkov, Dmitry Vukolov, James Stuber, Simon Woodruff, Influence of stray light on visible spectroscopy for the scrape-off layer in ITER, Plasma Phys. Control. Fusion 55 (8) (2013) 085020.
[6] S. Kajita, E. Veshchev, R. Barnsley, M. Walsh, Usage of ray tracing transfer matrix to mitigate the stray light for ITER spectroscopy: Usage of ray tracing transfer matrix to mitigate the stray light for ITER spectroscopy, Contrib. Plasma Phys. 56 (9) (2016) 837–845.
[7] M.-H. Aumeunier, M. Kočan, R. Reichle, E. Gauthier, Impact of reflections on the divertor and first wall temperature measurements from the ITER infrared imaging system, Nucl. Mater. Energy 12 (2017) 1265–1269.
[8] Shin Kajita, Maarten De Bock, Manfred von Hellermann, Andrei Kukushkin, Robin Barnsley, Ray tracing analysis of stray light for charge exchange recombination spectroscopy on ITER, Plasma Phys. Control. Fusion 57 (4) (2015) 045009.
[9] A.B. Kukushkin, V.S. Neverov, A.G. Alekseev, S.W. Lisgo, A.S. Kukushkin, Synthetic H-alpha diagnostics for ITER: Inverse problems and error estimations for strong non-Maxwellian effects and intense divertor stray light, Fusion Sci. Technol. 69 (3) (2016) 628–642.
[10] Shin Kajita, Marie-Helene Aumeunier, Eiichi Yatsuka, Andrey Alekseev, Evgeny Andreenko, Alexander Kukushkin, Vladislav Neverov, Martin Kocan, Michele Bassan, Evgeny Veshchev, Maarten De Bock, Robin Barnsley, Andrei Kukushkin, Roger Reichle, Michael Walsh, Effect of wall light reflection in ITER diagnostics, Nucl. Fusion 57 (11) (2017) 116061.
[11] Shin Kajita, Gilles Passedat, Roger Reichle, Ray tracing study of ITER in-vessel lighting system, Fusion Eng. Des. 160 (2020) 111787.
[12] M. Tomes, M. Carr, A. Meakins, M. Sos, P. Bohm, P. Bilkova, M. Imrisek, F. Jaulmes, I. Borodkina, J. Hecko, M. Hron, R. Panek, Thomson scattering synthetic diagnostic module for the Cherab framework, Rev. Sci. Instrum. 92 (5) (2021) 053532.
[13] M. Carr, A. Meakins, S.A. Silburn, J. Karhunen, M. Bernert, C. Bowman, A. Callarelli, P. Carvalho, C. Giroud, J.R. Harrison, S.S. Henderson, A. Huber, B. Lipschultz, T. Lunt, D. Moulton, F. Reimold, ASDEX Upgrade Team, JET Contributors, MAST-Upgrade Team, EUROfusion MST1 Team, Physically principled reflection models applied to filtered camera imaging inversions in metal walled fusion machines, Rev. Sci. Instrum. 90 (4) (2019) 043504.
[14] M. Ben Yaala, M.-H. Aumeunier, R. Steiner, M. Schönenberger, C. Martin, M. Le Bohec, C. Talatizi, L. Marot, E. Meyer, Bidirectional reflectance measurement of tungsten samples to assess reflection model in WEST tokamak, Rev. Sci. Instrum. 92 (9) (2021) 093501.
[15] M. Brank, R.A. Pitts, G. Simič, P. Lamalle, M. Kocan, F. Köchl, Y. Gribov, V. Polli, L. Kos, Assessment of plasma power deposition on the ITER ICRH antennas, Nucl. Mater. Energy 27 (2021) 101021.
[16] Hiroki Natsume, Shin Kajita, Vladislav S. Neverov, Radmir I. Khusnutdinov, Evgeny Veshchev, Maarten De Bock, Alexei R. Polevoi, Hirohiko Tanaka, Noriyasu Ohno, Hiroaki Ogawa, Sin-iti Kitazawa, Computer tomography on divertor impurity monitor for ITER with minimizing errors in a logarithmic scale, Plasma Fusion Res. 16 (2021) 2405019.
[17] A. Meakins, M. Carr, Raysect Python Raytracing Package, Zenodo, 2017.
[18] D. Guarnera, G.C. Guarnera, A. Ghosh, C. Denk, M. Glencross, BRDF representation and acquisition, Comput. Graph. Forum 35 (2) (2016) 625–650.
[19] M.-H. Aumeunier, M. Le Bohec, R. Brunet, A. Juven, M. Adel, X. Artusi, R. Miorelli, C. Reboud, F. Rigollet, Development of inverse methods for infrared thermography in fusion devices, Nucl. Mater. Energy 33 (2022) 101231.
[20] M. Houry, M.H. Aumeunier, C. Pocheau, X. Courtois, Ch. Dechelle, L. Dubus, E. Grelier, Th. Loarer, R. Mitteau, V. Moncada, H. Roche, The wide-angle infrared diagnostic for the first wall monitoring of the WEST tokamak, Fusion Eng. Des. 186 (2023) 113362.
[21] Hiroki Natsume, Kunpei Nojiri, Shin Kajita, Tomohiko Ushiki, Tatsuo Sugie, Sin-iti Kitazawa, Takanori Kikuchi, Tomohiro Yokozuka, Hirohiko Tanaka, Noriyasu Ohno, Takaki Hatae, Measurement of the bidirectional reflectance distribution function of tungsten surface sputtered in argon plasma, Plasma Fusion Res. 17 (2022) 2405041.
[22] Hiroki Natsume, Kunpei Nojiri, Shin Kajita, Makoto Fukuda, Tomohiko Ushiki, Hirohiko Tanaka, Tatsuo Sugie, Sin-iti Kitazawa, Takanori Kikuchi, Tomohiro Yokozuka, Noriyasu Ohno, Koichiro Ezato, Takaki Hatae, Bidirectional reflectance distribution function of recrystallized tungsten mono-block exposed to cyclic heat loading, Nucl. Mater. Energy 33 (2022) 101243.
[23] Bruce Walter, Stephen R. Marschner, Hongsong Li, Kenneth E. Torrance, Microfacet models for refraction through rough surfaces, in: Proceedings of the 18th Eurographics conference on Rendering Techniques, 2007, pp. 195–206.
[24] J. Gaspar, Y. Corre, F. Rigollet, M.-H. Aumeunier, E. Bernard, S. Brezinsek, X. Courtois, R. Dejarnac, M. Diez, L. Dubus, N. Ehret, N. Fedorczak, M. Firdaouss, M. Houry, M. Le Bohec, T. Loarer, C. Martin, V. Moncada, P. Moreau, C. Pocheau, P. Reilhac, E. Tsitrone, the WEST Team, Overview of the emissivity measurements performed in WEST: in situ and post-mortem observations, Nucl. Fusion 62 (9) (2022) 096023.
[25] C. Amra, Light scattering from multilayer optics I tools of investigation, J. Opt. Soc. Amer. A 11 (1) (1994) 197.
[26] Claude Amra, Michel Lequime, Myriam Zerrad, Electromagnetic Optics of Thin-Film Coatings: Light Scattering, Giant Field Enhancement, and Planar Microcavities, first ed., Cambridge University Press, 2020.

[27] Petr Beckmann, Andre Spizzichino, The scattering of electromagnetic waves from rough surfaces, 1987.
[28] Gregory J. Ward, Measuring and modeling anisotropic reflection, ACM SIGGRAPH Comput. Graph. 26 (2) (1992) 265–272.
[29] H.E. Bennett, J.O. Porteus, Relation between surface roughness and specular reflectance at normal incidence, J. Opt. Soc. Amer. 51 (2) (1961) 123.
[30] Michael G. Dittman, K-correlation power spectral density and surface scatter model, in: Optical Systems Degradation, Contamination, and Stray Light: Effects, Measurements, and Control II, vol. 6291, SPIE, 2006, pp. 226–237.
[31] R. Gavrila, A. Dinescu, D. Mardare, A power spectral density study of thin films morphology based on AFM profiling, Romanian J. Inf. Sci. Technol. 10 (3) (2007) 291–300.
[32] James E. Harvey, Narak Choi, Andrey Krywonos, Scattering from moderately rough interfaces between two arbitrary media, in: Optical System Contamination: Effects, Measurements, and Control 2010, 7794, SPIE, 2010, pp. 218–228.
[33] Jiří Vohánka, Václav Šulc, Ivan Ohlídal, Miloslav Ohlídal, Petr Klapetek, Optical method for determining the power spectral density function of randomly rough surfaces by simultaneous processing of spectroscopic reflectometry, variable-angle spectroscopic ellipsometry and angle-resolved scattering data, Optik 280 (2023) 170775.
[34] F.E. Nicodemus, J.C. Richmond, J.J. Hsia, I.W. Ginsberg, T. Limperis, Geometrical considerations and nomenclature for reflectance, Technical Report NBS MONO 160, National Bureau of Standards, Gaithersburg, MD, 1977, Edition: 0.
[35] M.F. Modest, Radiative Heat Transfer, third ed., Academic Press, New York, 2013.
[36] James F. Blinn, Models of light reflection for computer synthesized pictures, in: Proceedings of the 4th Annual Conference on Computer Graphics and Interactive Techniques, SIGGRAPH '77, Association for Computing Machinery, New York, NY, USA, 1977, pp. 192–198.
[37] Eric P. Lafortune, Yves D. Willems, Using the modified phong reflectance model for physically based rendering, 1994, p. 19.
[38] Bui Tuong Phong, Illumination for computer generated pictures, Commun. ACM 18 (6) (1975).
[39] Elham Kalantari, Yusuf Eshqi Molan, Analytical BRDF model for rough surfaces, Optik 127 (3) (2016) 1049–1055.
[40] Xiaozhou Li, Jingjing Liu, Xuelin Li, Dewei Qi, Guangyuan Wu, Research on optical model for microfacet reflectance lightness of stereo paper product surface with BRDF, Optik 242 (2021) 167337.
[41] R.L. Cook, K.E. Torrance, A reflectance model for computer graphics, ACM Trans. Graph. 1 (1) (1982) 7–24.
[42] Hiroki Natsume, Mickaël Le Bohec, Roland Steiner, Marwa Ben Yaala, Marie-Hélène Aumeunier, Laurent Marot, Shin Kajita, Hirohiko Tanaka, Effect of beryllium topography on BRDF measurements, Opt. Mater. 147 (2024) 114715.
[43] S. Feng, H. Natsume, S. Kajita, E. Li, R. Yasuhara, M. Tokitani, et al., Novel optical diffuser based on fiberform nanostructure by efficient plasma route, Optica Open (2023).
[44] Juan Irizar, Dr Bernd Harnisch, BRDF prediction using surface micro-roughness measurements, in: Proc. International Conference on Space Optical Systems and Applications, ICSOS, 2012.
[45] James E. Harvey, Andrey Krywonos, John C. Stover, Unified scatter model for rough surfaces at large incident and scatter angles, in: Angela Duparré, Bhanwar Singh, Zu-Han Gu (Eds.), in: Advanced Characterization Techniques for Optics, Semiconductors, and Nanotechnologies, vol. 6672, SPIE, International Society for Optics and Photonics, San Diego, CA, 2007.
[46] M. Minissale, C.L. De Canonville, C. Pardanaud, B. Butoi, R. Bisson, L. Gallais, The role of defects, deuterium, and surface morphology on the optical response of beryllium, Nucl. Fusion 62 (5) (2022).
[47] Villads Egede Johansen, Preparing the generalized Harvey-Shack rough surface scattering method for use with the discrete ordinates method, J. Opt. Soc. Amer. A 32 (2) (2015) 186–194, Publisher: Optica Publishing Group.
[48] C. Cupak, P.S. Szabo, H. Biber, R. Stadlmayr, C. Grave, M. Fellinger, J. Brötzner, R.A. Wilhelm, W. Möller, A. Mutzke, M.V. Moro, F. Aumayr, Sputter yields of rough surfaces: Importance of the mean surface inclination angle from nano- to microscopic rough regimes, Appl. Surf. Sci. 570 (2021) 151204.
[49] P.S. Szabo, C. Cupak, H. Biber, N. Jäggi, A. Galli, P. Wurz, F. Aumayr, Analytical model for the sputtering of rough surfaces, Surfaces Interfaces 30 (2022) 101924.
[50] Xiao D. He, Kenneth E. Torrance, François X. Sillion, Donald P. Greenberg, A comprehensive physical model for light reflection, ACM SIGGRAPH Comput. Graph. 25 (4) (1991) 175–186.
[51] Hiroshi Ohno, One-shot color mapping imaging system of light direction extracted from a surface BRDF, OSA Continuum 3 (12) (2020) 3343–3350, Publisher: Optica Publishing Group.
[52] Hiroshi Ohno, Takahiro Kamikawa, One-shot BRDF imaging system to obtain surface properties, Opt. Rev. 28 (6) (2021) 655–661.